WIND ENERGY
Wind Energ. (2011)
Published online in Wiley Online Library (wileyonlinelibrary.com). DOI: 10.1002/we.437

PAPER PRESENTED AT AWEA WINDPOWER 2010

Structural health monitoring of wind turbines: method and application to a HAWT

Douglas Adams[1], Jonathan White[2], Mark Rumsey[2] and Charles Farrar[3]

1 School of Mechanical Engineering, Purdue University, West Lafayette, Indiana, USA
2 Wind and Water Technologies, Sandia National Laboratory, Albuquerque, New Mexico, USA
3 Engineering Institute, Los Alamos National Laboratory, Albuquerque, New Mexico, USA

ABSTRACT

Structural health monitoring in the context of a Micon 65/13 horizontal axis wind turbine was described in this paper as a process in statistical pattern recognition. Simulation data from a calibrated model with less than 8% error in the first 14 natural frequencies of vibration was used to study the operational response under various wind states as well as the effects of three types of damage in the blade, low speed shaft and yaw joint. It was shown that vertical wind shear and turbulent winds lead to different modal contributions in the operational response of the turbine suggesting that the sensitivity of operational data to damage depends on the wind loads. It is also shown that there is less than a 4% change in the wind turbine natural frequencies given a 25% reduction in the stiffness at the root of one blade. The modal assurance criterion was used to analyse the corresponding changes in modal deflections, and this criterion exhibited nearly orthogonal changes because of the three damage scenarios suggesting that the modal deflection determines which damage is observable at a given frequency for a given wind state. The` modal contribution is calculated as a damage feature, which changes as much as 100% for 50% reductions in blade root stiffness, but only the blade damage is detected using this feature. Operational data was used to study variations in the forced blade response to determine the likelihood that small levels of damage can be detected amidst variations in wind speed across the rotor plane. The standard deviation in measured data was shown to be smallest for the span and edge-wise measurements at 1P due to gravity, which provides the dominant forcing function at this frequency. A 3% change in the response in the span and edge-wise directions because of damage is required to detect a change of three standard deviations in contrast to the 90% change in flap direction response that is required to detect a similar change because of damage. The dynamic displacement in the span direction is then used to extract a damage feature from the simulation data that provides the ability to both locate and quantify the reduction in stiffness in the blade root. Copyright © 2011 John Wiley & Sons, Ltd.

KEYWORDS

structural health monitoring; horizontal axis wind turbine; vibrations; accelerometers

Correspondence

D. Adams, School of Mechanical Engineering, Purdue University, 1500 Kepner Drive, West Lafayette, Indiana, USA.
E-mail: deadams@purdue.edu

Received 23 June 2010; Revised 30 August 2010; Accepted 4 October 2010

1. INTRODUCTION

1.1. Motivation

Wind turbine manufacturers, owners and operators could benefit financially from structural health monitoring (SHM) technology, which provides an indication of the reliability of each wind turbine throughout its 10–30 year lifecycle. The term 'health' encompasses the loading, damage and operational capability (i.e. life at the rated performance) of a turbine. Each turbine is comprised of subsystems such as the rotor, drive train, generator and tower, and components such as the blades, bearings, yaw joints and shafts. The operational reliability, and, more pertinent to operation and maintenance, the uncertainty in reliability of a complex system like a wind turbine is dictated by the loading and condition at the component level.[1] Whereas the discipline of design focuses on the loading, performance, failure modes and reliability of a

population of wind turbines and its subsystems, the discipline of SHM focuses on individual wind turbines at the component level. If the loading and health of individual wind turbines could be quantified, the maintenance, operation and control of each turbine could be tailored to maximize uptime by increasing the mean time between inspections and other factors that influence uptime.

For instance, scheduled maintenance requiring approximately 24 h per turbine is performed twice per year on most utility horizontal axis wind turbines (HAWTs). Unscheduled maintenance is approximately 500% more costly to conduct requiring 130 h per turbine.[2] It is envisioned that SHM will provide maintainers with actionable information that they can utilize to schedule maintenance ahead of time to avoid more costly unscheduled maintenance actions. Furthermore, manufacturers could use health information about loads and the damage correlated with these loads to improve wind turbine designs, manufacturing and quality control processes, and shipping and installation methods. For the wind farm owners and operators, knowledge of the health of the entire system of wind turbines as well as the health of the local electrical utilities could be of great economic benefit from an energy production and delivery point of view. SHM could also potentially enable designers to reduce the weight of rotors and drive trains by replacing conservative design assumptions with automatic state awareness and control measures.[3]

As a specific example of a potential damage mechanism that SHM can address, consider a blade pitch actuator or bearing that exhibits unusually large amounts of hysteresis resulting in a bias error in the desired angle of attack for that blade. Such a blade's loading and health, as well as the health of the drive train with which that blade interacts, could be compromised. Wind farm operators could compare stored historical loads estimates of that individual turbine, particularly for severe loads, to the assumed design loads to assess the potential impacts on the turbine's life. If the mechanical defect in the pitch drive system could be detected, operators could also deploy maintenance resources in a proactive manner to correct the mechanical defect and avoid losses in energy capture or downtime because of more extensive unscheduled maintenance that could be required in the future. In addition, operators could pitch the other two blades to temporarily suppress asymmetric loads to the rotor and drive train that are partially responsible for causing the growth of fatigue damage to allow for the necessary parts to be ordered in a timely manner. Performance-based logistics could then be used by wind turbine maintainers to place orders for parts, which often have relatively long delivery lead times.

1.2. Scope and objectives

This paper provides an overview of the SHM method and its application to a horizontal axis wind turbine (HAWT). Technical approaches in the acquisition, processing and interpretation of operational vibration data are emphasized. Because only one turbine was tested in a given wind regime, and these tests were non-destructive in nature, a simulation model of the Micon 65/13 turbine was used to enable several types of wind states, and hence loads, including vertical wind shear and turbulent winds, to be investigated. Several damages were also studied using this simulation model including damage in the yaw bearing, low-speed shaft bearing and blade root section. These components were selected for the damage investigation based on the reliability data discussed by Hahn, Durstewitz and Rohrig.[2] These authors analysed data from 1500 utility HAWTs to identify the most frequent mechanical damages. Hydraulic pitch actuators and bearings had a 25% chance of becoming damaged once per year followed closely by yaw drives and bearings and rotor blades, which had a 20% chance of experiencing damage, and gearboxes, which had an 18% chance of becoming damaged. Damages in the simulations in this paper on SHM were introduced by reducing the stiffness in the root of the blade (to simulate either blade damage or pitch bearing damage), the yaw bearing (to simulate either yaw bearing wear or yaw drive damage) and the low-speed shaft (to simulate either shaft or main bearing damage). Damage in the low-speed drivetrain can lead to a whirling motion and imbalanced forces that are contributing causes of gearbox damage. By conducting time-marching simulations of the HAWT model with and without damage, the simulated data was then analysed using cyclic averaging and vibration analysis to determine if the changes because of damage could be realistically discerned in the context of real-world sources of variability in experimental data because of fluctuations in wind speed, direction and spectral content.

The specific objectives of the paper were as follows:

- A full-turbine model of a HAWT was reviewed including the model updating procedure and modal vibration test data from the turbine that was used to update the model.
- The measurement system used to acquire modal vibration and operating data from the HAWT was briefly described, and forced responses in the simulated and experimental datasets were compared.
- A four-step SHM process was demonstrated to identify operating loads and three types of damage using both simulated and experimental data. The simulated forces and responses of the turbine were analysed for vertical wind shear and turbulent wind cases to assess the contributions of 14 modes of vibration. Data was cleansed using a sample and hold filter to fill in gaps in the data because of signal dropout. Features for damage detection were extracted to maxi-

mize the probability of detection amidst variations in aerodynamic loading because of changes in wind speed. Modal natural frequencies and deflection shapes of the model with and without simulated damages were analysed to determine the physical sensitivity of the turbine rotor blade responses to damage.

Operational data was then analysed to extract statistical moments, which were used to determine the percent change in blade responses that would be required to detect a significant change because of each of the three damage mechanisms that were being investigated.

1.3. Method

SHM is a discipline that aims to identify the health of an engineered system throughout its lifecycle.[4] The health state of a system such as a wind turbine changes with time and is a function of the initial state of the system (quality) as well as the loads that act on the system (e.g. extreme loads, cyclic loads, environmental conditions). Therefore, SHM methodologies are often applied in the design phase, during durability testing, during shipping and installation (of blades and drive train subsystems), and in operation to take full advantage of all lifecycle data.[5] Condition monitoring (CM) of rotating machinery like wind turbines utilizes passive response data collected and analysed locally along the drivetrain.[6] One can think of CM as a subset of SHM because local damage in rotating components such as bearings,[7] shafts and motors[8] are usually directly sensed in CM whereas SHM seeks to locate, as well as detect, damage mechanisms globally within various wind turbine components. SHM also generally involves the implementation of both passive sensing of the response because of the operational loads[9] and active sensing of the response through driven actuators[10–12] to extract relevant data for damage identification. CM is a more mature field than SHM because there are many commercially available CM systems, whereas there are only a few commercially available SHM systems. The focus in this paper was on the use of passive sensing of wind turbine operating acceleration response in one of the rotor blades to identify the static and dynamic response of the blade and damage to the blade, low-speed shaft and yaw joint. It was envisioned here that damage prognosis could be subsequently applied following the method in this paper to predict the remaining useful life of individual components (e.g. bearings, gears and lubricant) within the turbine based on their specific loading histories, projected future loadings and estimated damage levels. Other SHM-related tasks in the context of a wind turbine include nondestructive evaluation of manufactured parts such as gears and composite blades for quality control[13] and statistical process control to monitor the phase of energy production of individual wind turbines and entire wind farms that supply electricity to the grid.[14,15]

A four-step process that equates SHM to a problem in pattern recognition was used here to demonstrate the SHM method on simulation data and experimental data from a Micon 65/13 turbine. This HAWT is described in detail by Jones, Sutherland and Neal.[16] The SHM process is outlined below in the context of this HAWT and was described by Sohn *et al.*[17]

First, an *operational evaluation* was conducted to determine how the loading environment affects the wind turbine rotor blade response measurements for the Micon 65/13 turbine. The frequency content in the passive vibration response data from an operational blade directly influences the analyst's ability to detect damage to the blade, low-speed shaft or yaw joint. The reason that some damage mechanisms can be detected using operational vibration measurements whereas other damages cannot be detected is because of the modal nature of forced vibration data. The forced vibration response for a certain wind loading condition was assumed to be comprised of the modes of vibration as illustrated in Figure 1 and expressed in equation (1):

$$\frac{X_p(\omega)}{F_q(\omega)} = \sum_{r=1}^{N} \frac{Q_r \psi_{pr} \psi_{qr}}{j\omega - \lambda_r} + \frac{Q_r^* \psi_{pr} \psi_{qr}}{j\omega - \lambda_r^*} \tag{1}$$

where X_p and F_q denoted the blade response at degree of freedom p and forcing function at degree of freedom q as a function of frequency, respectively, Q_r was the modal scale factor for mode of vibration r, λ_r was the modal frequency for mode r, and ψ_{pr} was the modal deflection of degree of freedom p for mode r. It was assumed in equation (1) that N modes of vibration were sufficient to describe the turbine dynamic response. In this paper, 14 modes of vibration were used to describe the turbine response up to 16 Hz. The 1st symmetric flap mode of vibration of the wind turbine rotor was illustrated in Figure 1 as an example of the possible modes of vibration that could be excited by the operational loads applied to the wind turbine. This particular mode of vibration did not involve significant deflection of the low-speed shaft or the yaw joint suggesting that operational response data in the vicinity of this modal frequency of vibration would not enable the analyst to detect damage to these components of the wind turbine.

Second, *data acquisition and cleansing* was performed to produce advantageous inputs that were to be processed by damage identification algorithms. For instance, data from the fixed and rotating reference frames (on the hub) might

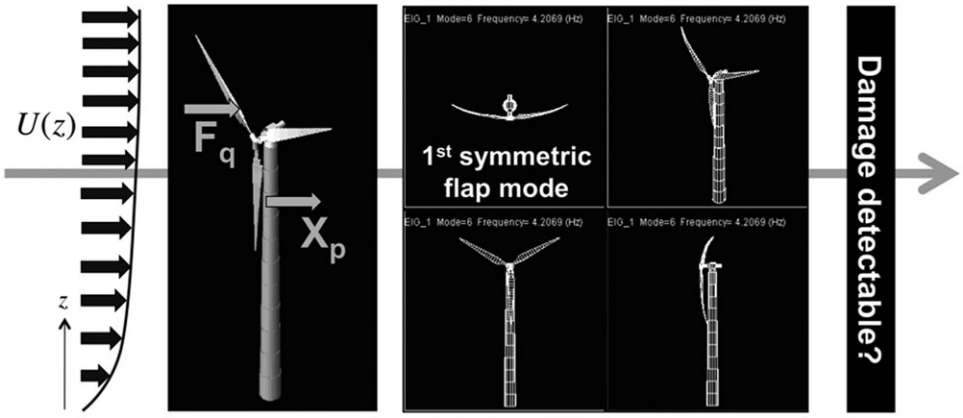

Figure 1. Process of vibration-based structural health monitoring to detect damage in a wind turbine, where the operational loading influences modes of vibration that are excited and, consequently, the ability to detect damages in the blade, low-speed shaft and yaw joint.

contain dropouts that must be filled in using an appropriate interpolation algorithm such as sample-and-hold or autoregressive filters. In a wind turbine, it was also appropriate to use tachometer sensors on the low speed shaft to synchronize the analysis of time histories from the operating blade using angle domain averaging. This process of converting response data from the time domain, in which accelerations vary with time, to the angle domain, in which accelerations vary with the angle of the low-speed shaft at the hub, and then performing averages using this converted data, aided in reducing the effects of frequency domain leakage. Synchronous signal processing also served to emphasize deterministic content in response data while de-emphasizing non-deterministic content because of the stochastic nature of wind loads. The deterministic content in response data was thought to be more associated with damage to turbine components. A high-pass filter was also applied to simulated data to isolate the contributions of modes of vibration.

Third, *feature extraction* algorithms were applied to the data to increase the sensitivity to damage and/or decrease the sensitivity to other factors such as variations in wind loads. The purpose of these algorithms was to extract quantitative or qualitative indices, which were sensitive to the health of particular components, e.g. bending stiffness of rotor blade in root section, bending stiffness of low-speed shaft and/or bearing or yaw joint bending stiffness. Indications of damage were obtained by performing feature comparisons. For example, the natural frequencies and mode shapes for the wind turbine were compared in the undamaged and damaged states. Percent differences in natural frequencies as well as modal assurance criterion (MAC) calculations for the modal vectors of the wind turbine were analysed in this paper to determine if these were potential features for damage detection. Likewise, the dynamic displacement in operation could be used as a feature for damage detection if the operating condition did not change with time. The potential of using the dynamic displacement attributed to the repetitive oscillating gravitational load on the blade of the rotor was investigated as a means of increasing the probability of detecting damage in the blade root.

Fourth, a *statistical model for discrimination* was developed to determine if observed changes in the extracted features from simulated data were statistically significant given variations in the features during normal operation that was measured experimentally. Inherent in this process is the need for data normalization. In the context of SHM, data normalization refers to the process of separating changes in a sensor reading caused by varying operational and environmental conditions from the changes caused by damage. Data normalization can be performed in either hardware or software, and typically some combination of these approaches is used. Ideally, this process is carried out with direct measures of the sources of variability (e.g. temperature, wind speed, wind direction). This paper considered the use of an along-wind wind speed measurement to normalize the blade response data to reduce variability in dynamic response features. Experimental data was analysed to attach a level of confidence to a diagnosis that damage was present by analysing changes in the damage feature with respect to normal statistical variations in measured data. In the absence of such direct measures of variability, machine-learning algorithms could be used to model the influence of such sources of variability on the damage detection process given data from known structural conditions that were acquired under the variable conditions.[18] For example, if the wind speed varied peak-to-peak by a large amount for a particular turbine, then a machine learning approach referred to as non-linear principle component analysis (a.k.a. auto-associative neural networks) could 'learn' how this varying wind speed influences the feature even without a measure of the speed. This machine-learning algorithm could then be used to determine if changes in measured features are statistically significant in the context of these wind speed variations. Other sources of variation include temperature and humidity changes, which affect the properties of rotor blades and lubricants.

1.4. Related literature

The literature in SHM was categorized according to the two main subsystems of wind turbines: rotor blades along with other primary structures (tower, foundation, etc.) and drive train. However, a few general overview papers were also found in the literature. Ciang, Lee and Bang[3] provided a review of SHM as it applied to wind turbines and also summarized relevant damage mechanisms in wind turbines with an emphasis on blade and tower structures. Liu, Tang and Jiang[19] also provided a focused review of SHM methods being investigated in China.

SHM applied to wind turbine blades has been studied by a number of researchers. Ghoshal, Sundaresan, Schulz and Pai[20] described research focused on SHM of composite wind turbine blades, and Sundaresan *et al.*[21] provided a detailed review of SHM based on the use of stress wave measurements that were recorded during static blade testing at the National Renewable Energy Laboratory. These measurements were correlated with the onset of visible damage to the blade and grew in intensity as the damage evolved. A similar approach for monitoring damage during static blade tests using a network of acoustic emission sensors was described by Krikera *et al.*.[22] A relatively comprehensive review of SHM and non-destructive testing methods applied to wind turbine blades was also provided by Lading *et al.*. [23] Corey, Grisso and Inman[24] described their study of electromechanical impedance-based sensing as a means of detecting blade damage during static testing of a blade to failure. White *et al.*[11] demonstrated passive impact load estimation and active damage detection methods based on the use of acceleration sensors that recorded the dynamic response of a TX-100 rotor blade during static testing performed by the Sandia National Laboratory at the National Renewable Energy Laboratory. An overview of SHM techniques based on vibration, acoustic emission and impedance measurements taken during a wind turbine blade static test was also provided by Rumsey and Paquette.[25] Schroeder *et al.*[26] demonstrated the use of fibre Bragg grating strain sensors for monitoring the loads applied to the rotor blades of a utility scale wind turbine. White, Adams, Rumsey and Zayas[9] also demonstrated the use of capacitive acceleration sensors along with physics-based algorithms to estimate the deflection and loading experienced by a rotor blade in a model-based simulation and in experiments on a 115 kW wind turbine.

Several review papers that described sensing techniques and algorithms for CM of drive train components like bearings and gears in utility scale wind turbines were found. Walford and Roberts[27] and Hyers *et al.*[23] provided detailed reviews of the methods for CM of critical drive train components. These authors also described the physics of failure involved in the development of drive train faults. Hameed *et al.*[28] also provided a review that was focused on the algorithms for fault detection in CM systems for wind turbines.

None of this prior work focused on the use of capacitive acceleration measurements as a means of measuring the response of a rotor blade for the purpose of detecting damage in the blade. Also, prior work in CM of wind turbines has utilized sensors installed on the drive train for fault detection; however, this paper explores the potential of using blade operational response measurements to detect faults in the drive train (low-speed shaft) and nacelle (yaw joint). This prior work also largely emphasized the monitoring of individual blades during quasi-static testing as opposed to when the blade was operating on a rotor hub, which involves coupling among the blades and across the turbine (driveline and tower). This paper addresses the potential of using such measurements in an operating turbine (both in a simulation model and in experiments) to detect damage for the purpose of SHM.

2. SIMULATION MODEL

SHM was demonstrated in this paper for a Micon 65/13 fixed speed, pitch and yaw turbine with CX-100 rotor blades shown in Figure 2(a). The report by Jones, Sutherland and Neal[16] described this turbine and some of the instrumentation available for use in the experimental portion of the work being presented here. The turbine was installed at the US Department of Agriculture Conservation and Production Research Laboratory in Bushland, TX. A smart sensored blade was installed on the rotor hub and tested by the Sandia National Laboratory. In addition to the in-blade single axis (PCB 3711) and triaxial PCB Piezotronics capacitive acceleration sensors (PCB 3713) that were integrated within one of the blades as shown in Figure 2(b), drive train rotational position and power sensors and wind inflow field arrayed sensors produced data that was available for post-processing. The positions of these accelerometers were chosen in order to avoid nodes of vibration of the rotor blade assuming a clamped boundary condition at the root. Sensor locations were also optimized in previous research according to criteria that were prescribed on the accuracy of the estimated blade deflections[9]).

A lumped-parameter dynamic model was developed in ADAMS© using the FAST2ADAMS routine that was constructed based on a model originally developed in the FAST (Fatigue, Aerodynamics, Structures, and Turbulence) environment. This model utilized estimates of the full-field stochastic aerodynamic loads generated with the Aerodyn software. The mass and elastic parameters of the model were updated as discussed in detail by White, Adams and Rumsey[29] to match experimentally acquired modal vibration test data including both natural frequencies and modal deflection shapes. Only modest updates to the model parameters like the blade modulus of elasticity were made to avoid over fitting of the

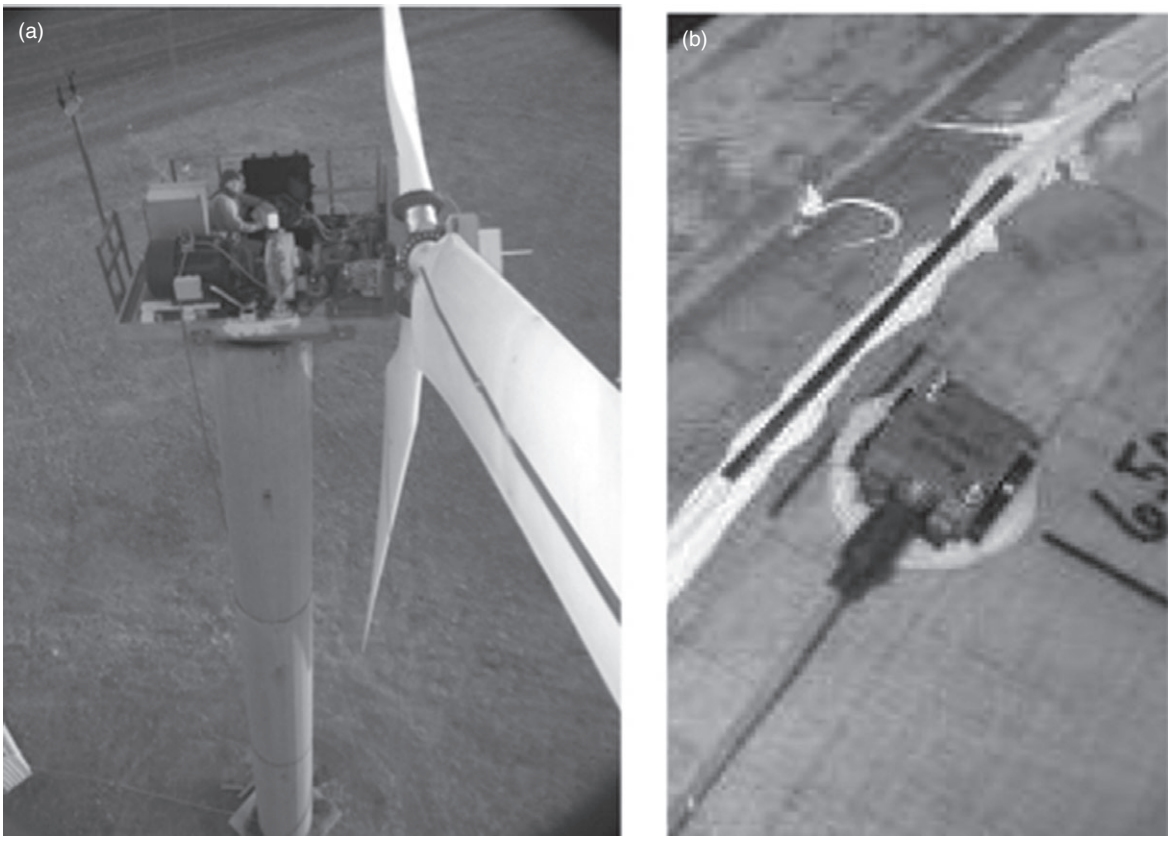

Figure 2. (a) Micon 65/13 wind turbine with 10 capacitive accelerometers like the one in (b) installed in the blade and mounted to the hub, and a wireless data acquisition box on hub.

experimental data. The blade modulus and density were adjusted slightly to achieve a good match between the modal test results for the 9 m composite rotor blade (see Figure 3(a)) and the simulated results using 20 beam elements to model each of the three blades. Modal analysis experiments were performed on the rotor blade with free–free and cantilevered boundary conditions. The free–free modal frequencies and shapes were used to evaluate and update the distribution of stiffness and mass in the blade model. The updating was mostly focused on the outboard 75% of the span because the large mass at the blade root acted as an inertial mass boundary condition and limited the measured vibration magnitude in this region. The cantilevered modal test exercised the root area more significantly; therefore, the data from this experiment could be used to evaluate and update the inboard 25% stiffness. The accuracy of the model of the inboard 25% of the blade was critical to the overall turbine model accuracy because this portion of the blade (under quasi-static deflection) carried the majority of the load. Also, the tower foundation properties were adjusted so that the simulation model modal properties matched the experimental results for the tower reported by Simmermacher *et al.* (1999) (see Figure 3(b)). For the fully assembled wind turbine model, a two-stage process was used to update the model. In the first stage, an analytical model of the low-speed drive train (hub, shaft and bearings) was used to create a representative flexible low-speed shaft. In the second stage, a parametric sensitivity analysis was performed for the turbine yaw joint and used to update the six stiffness parameters that define the interaction between the tower and nacelle. These parameters were adjusted to reduce the difference between the simulated and experimentally estimated natural frequencies for the full turbine (see Figure 3(c)) into good agreement.

Figure 4 lists the first 14 natural frequencies that were estimated from the experimental modal impact test data collected on the full turbine. The percent difference between the simulated and experimental natural frequencies, when using the experimental estimate as the reference value, was plotted on the *x*-axis of the table. There was a maximum 3% difference with respect to the initial dynamic model parameters before model updating, the model after updating the low-speed shaft stiffness and the model after making both the low-speed shaft and yaw joint updates. The largest percent error was 8% for the second flap horizontal anti-symmetric mode of vibration down from an original error of 40% because of the lack

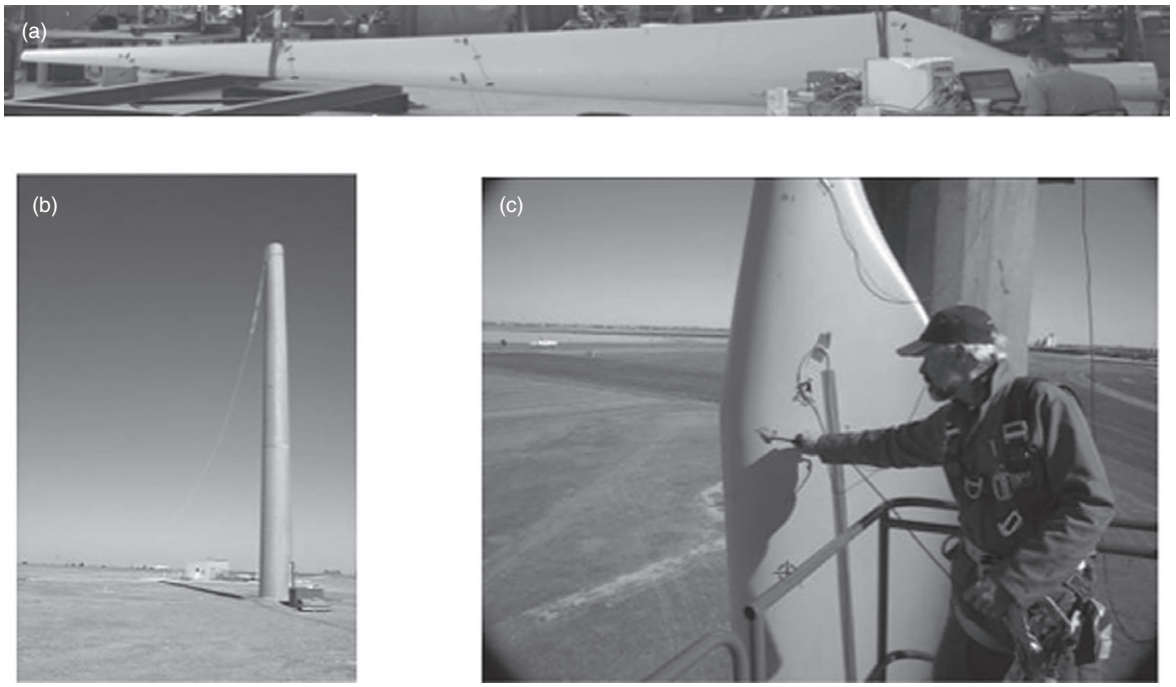

Figure 3. Experimental modal impact testing was performed on (a) an individual blade (b) the tower courtesy of Simmermacher *et al.* (1999) and (c) the fully assembled turbine to obtain natural frequency and mode shape estimates for use in updating the dynamic model.

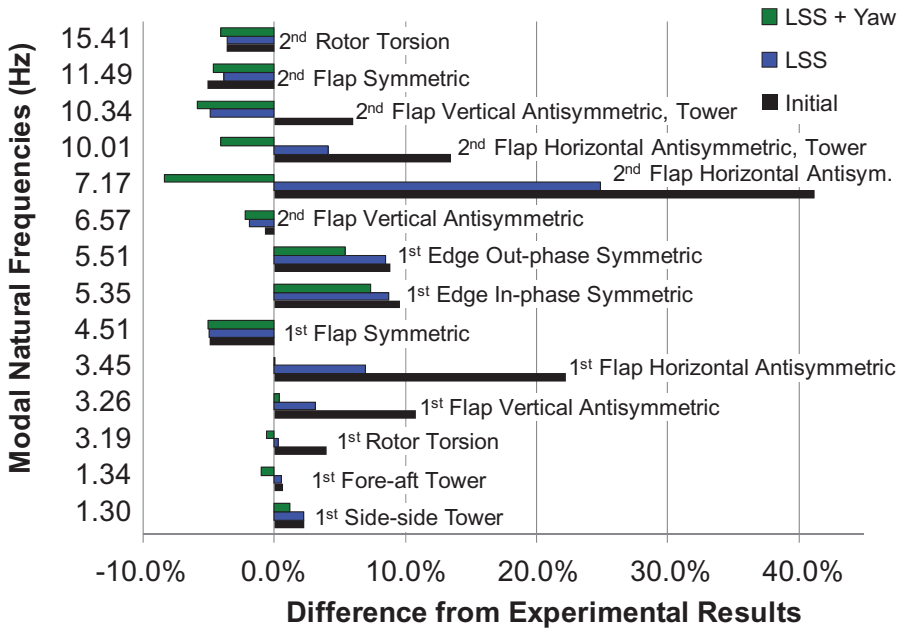

Figure 4. Percent difference between experimentally estimated undamped natural frequencies and simulated natural frequencies for the initial multi-body dynamics model (■), after update to low-speed shaft (■) and after final update to both shaft and yaw joint (■).

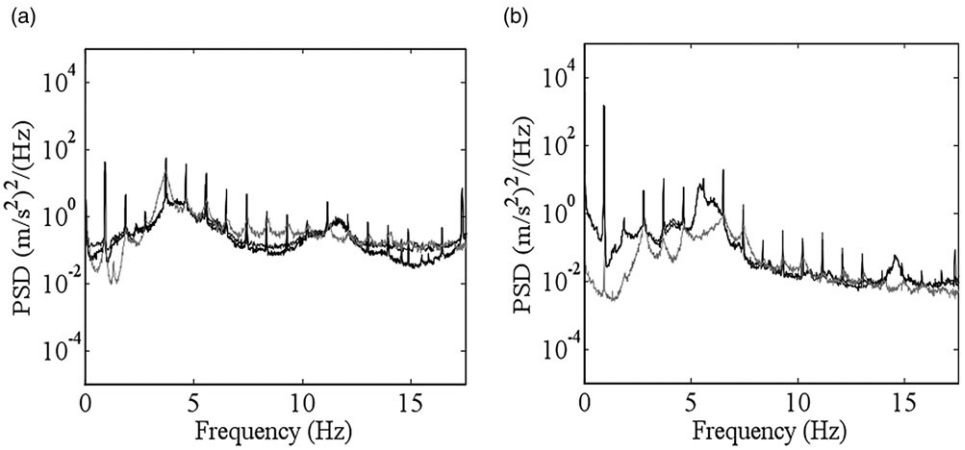

Figure 5. Power spectral density estimates for (a) flap and (b) edge-wise accelerations at 6.5 m span location of blade showing comparison between experimental measurements on the high-pressure and low-pressure sides of the blade (—) and simulated (—) data.

of flexibility in bending of the low-speed shaft. This updated model was used to conduct the simulations described in the remainder of the paper. Simulations were conducted using a 0.025 s time step to provide adequate time resolution to describe modes of vibration out to 20 Hz. Vertical wind shear was incorporated using the power law in equation (2) and class B turbulence was incorporated using the Kaimal distribution in equation (3):

$$U(z) = U(z_{hub}) \times \left(\frac{z}{z_{hub}} \right)^{\alpha} \tag{2}$$

$$\frac{fS_{Kaimal}(f)}{\sigma_k^2} = \frac{4fL_k/U_{hub}}{(1+6fL_k/U_{hub})^{5/3}} \tag{3}$$

where z was the distance from the base of the tower to the height of wind speed $U(z)$, z_{hub} = 23 m was the height of the hub, α = 0.2, and f was the frequency in Hz, U_{hub} = 15 m s^{-1} was the wind speed at the hub, σ^2_k = 2.36 m s^{-1} was the variance in the wind speed and L_k = 130 m was the integral scale parameter for the Kaimal distribution. Simulations discussed in this paper included the case of vertical wind shear for various mean wind speeds and the case where both vertical wind shear and class B turbulence were acting on the turbine.

Having already compared the experimental and simulated model natural frequencies in Figure 4, the operating forced responses from the experimental and simulation data were also compared as shown in Figure 5. Power spectral density estimates were shown in Figure 5 for (a) flap and (b) edge-wise accelerations at the 6.5 m span location of one blade of the rotor. The rotor speed was approximately 0.93 Hz in these plots. The overall trends of the experimental and simulated data were similar except for in the edge-wise acceleration response below 2.5 Hz. This error was believed to be caused by misalignment of the accelerometer installed within the smart blade, boundary conditions of the blade that were modelled using zero slope and relative deflection at the hub and un-modelled driveline dynamics. The experimental data was also generally higher at the peak frequencies corresponding to harmonics of the rotor speed. This difference was likely because of the use of a proportional viscous damping model in the simulation model. Despite these differences between the experimental and simulated operating data, it was assumed that the simulation results could be used to draw conclusions about the use of vibration data in the rotor blade for SHM.

3. SHM PROCESS

3.1. Operational evaluation

The operational evaluation of this wind turbine began by characterizing the nature of the wind loads that acted upon the rotor at the test site. For SHM damage detection, it was critical to determine the sensitivity of measured vibration data

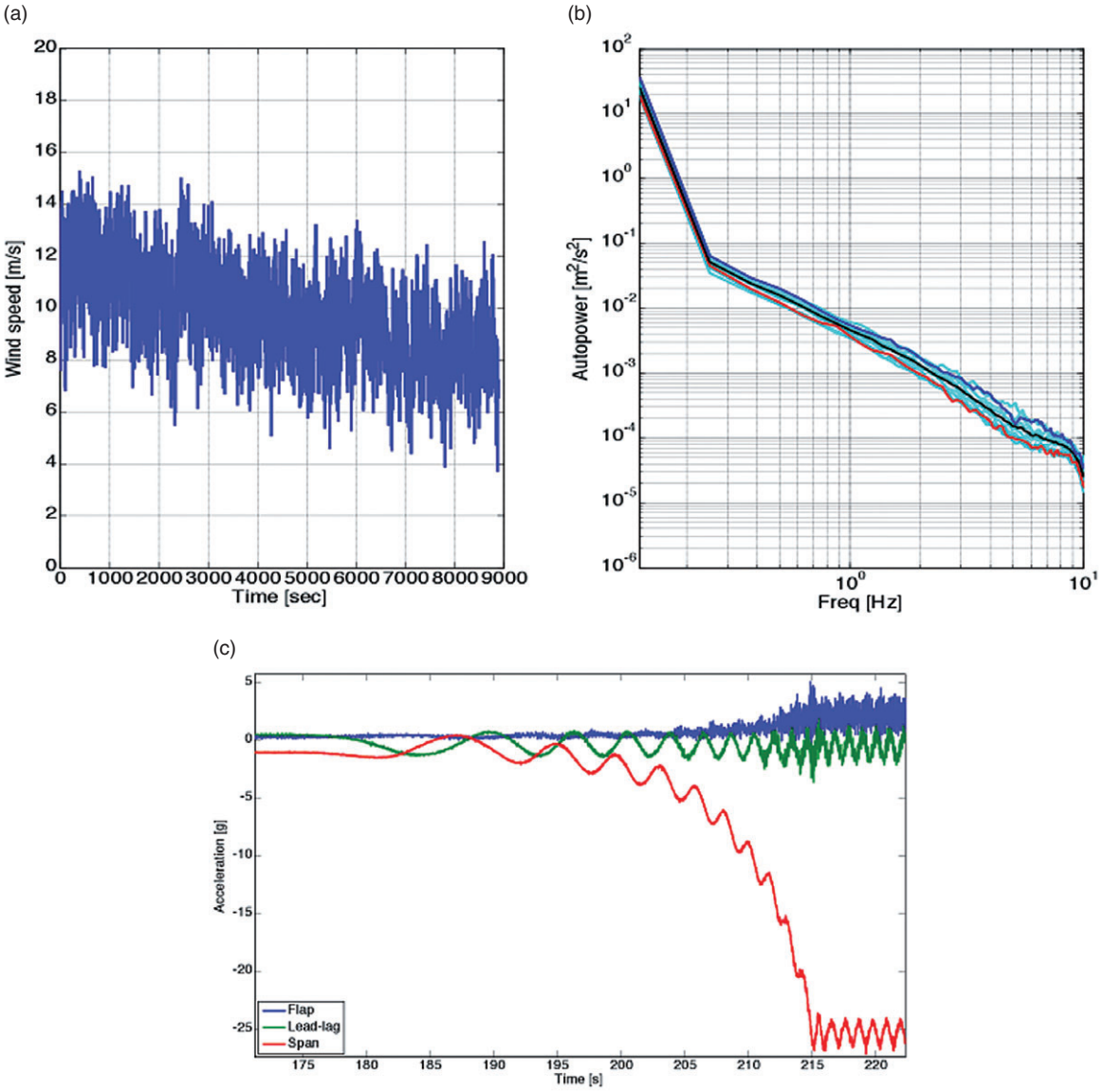

Figure 6. (a) Wind speed in turbine axis direction over 180 min period (b) autopower spectra of wind speed using 50% overlap processing and Hanning window for 180 min period (—), initial 18 min (—), intermediate periods (—) and final 18 min (—); and (c) start-up and steady state acceleration measurements at the 6.5 m span position along sensored blade for flap (—), edge-wise (—) and span (—) directions.

to damage. By measuring and understanding load data and combining this understanding with the feature sensitivity analysis obtained from the ADAMS turbine simulation model in a subsequent section, the feasibility of using operational response data to detect damage in the rotor, drive train and tower could be assessed. Figure 6(a) shows the wind speed measurement that was taken 1.5 rotor diameters upstream from the turbine at hub height in the along-wind (rotor axis) direction. This measurement indicated that the mean speed decreased steadily over a 3 h period. The autopower spectra shown in Figure 6(b) were estimated using 50% overlap averaging, which was applied to the entire 180 min dataset and also to 18 min sequential datasets to quantify the change in spectral content with time. A Hanning window was used to decrease the effects of leakage, and the blocksize for signal processing was chosen to correspond to six revolutions of the fixed-speed rotor. The spectral magnitudes above 0.2 Hz indicated that the dynamic components followed a random process that could be modelled using an exponential function as discussed by Saranyasoontorn, Manuel and Veers (2004), i.e. a straight line in log–log space. In subsequent simulations of this wind turbine, the relationship in equation (3) was

used to describe this wind spectrum. The autopower spectra all rolled off 60 dB by 10 Hz. This finding suggested that the simulation model and data analysis should focus on the dynamic response just beyond the 14th mode of vibration near 15 Hz according to Figure 4.

The evolution of the wind spectra in Figure 6(b) suggested that the dynamic loads were also decreasing in amplitude with time. This information was critical to the damage detection process in SHM because the data analysis needed to take into account this decay so that small changes in the turbine components could be diagnosed. Lastly, the response measurements acquired from a triaxial accelerometer (flap, lead-lag and span degrees of freedom) positioned at the 6.5 m span location along the sensored blade during start-up and steady state were plotted in Figure 6(c). These measurements could be used in future work to assess the potential of using both transient and steady response data to detect damage. It is often useful in SHM to process data during transient and steady regimes depending on the damage of interest because of different vibration frequencies that are excited in these two regimes.

To assess how the variation in wind loading illustrated in Figure 6(a),(b) affected the operational loading and vibration response of the CX-100 rotor blade, the ADAMS model was used to simulate the operational response. This data was then used to calculate the aerodynamic forces acting on the rotor blade. The contributions of the 14 modes of vibration to the overall operational response of the blade were also calculated for two different wind states, vertical wind shear and class B turbulence with wind shear, using the parameters given following equations (2) and (3). These modal contributions were critical to the task of SHM damage detection for the reason illustrated in Figure 1. The aerodynamic force spectral distributions acting along the span of the blade in the simulated wind shear and turbulent wind states for the 10 m s^{-1} mean wind speed were plotted in Figures 7(a),(b). These spectra were calculated using the angle domain resampling and averaging procedure described in a subsequent section of this paper. The force distribution in the case of vertical wind shear (Figure 7(a)) had strong components at one, two and three times per rotation with the strongest component at the rotational speed, with little broadband content. In contrast, the force distribution for turbulent wind exhibited strong components at 0 Hz, many harmonic frequencies of the rotational speed, and frequencies between those harmonics because of the stochastic nature of the turbulent wind state. These results suggested that the turbulent winds were exciting a larger number of modes of vibration compared with the vertical wind shear case.

To confirm this hypothesis, the modal contributions were calculated using the set of modal vectors as the basis functions with which to decompose the operational displacements of the simulated turbine degrees of freedom. This decomposition was formulated as follows using a coordinate transformation from physical to modal coordinates:

$$\{x(t)\} = [\Psi]\{p(t)\} \tag{4}$$

where the 14 columns of $[\Psi]$ were the modal vectors of the at-rest turbine, $\{x(t)\}$ was the vector of operational displacements and $\{p(t)\}$ was the vector of 14 modal coordinates or contributions. In the wind turbine simulation model or in the case when there are more measurement degrees of freedom than modes of vibration, equation (4) would be an overdetermined set of equations. These equations were solved by calculating the pseudoinverse of the matrix of modal vectors. After applying a 0.1 Hz cut-off high pass filter, the modal contributions that comprised the operational response for a wind state with vertical shear (equation (2)) were calculated using the pseudoinverse solution of equation (4). Then the root mean square values were calculated for each of the modal contributions. These mean contributions were plotted in

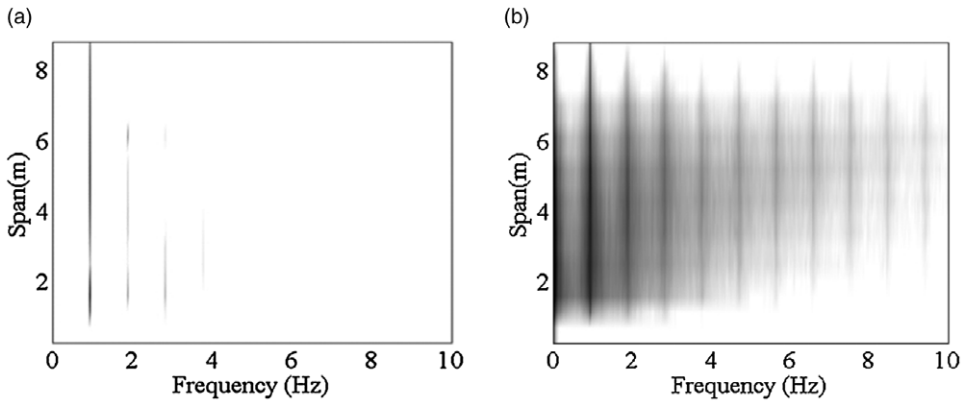

Figure 7. Force distribution along the span of one rotor blade using synchronous averaging in the angle domain (see Figure 10(a)) for (a) vertical wind shear and (b) class B turbulence with wind shear where dark colours indicate larger force amplitudes.

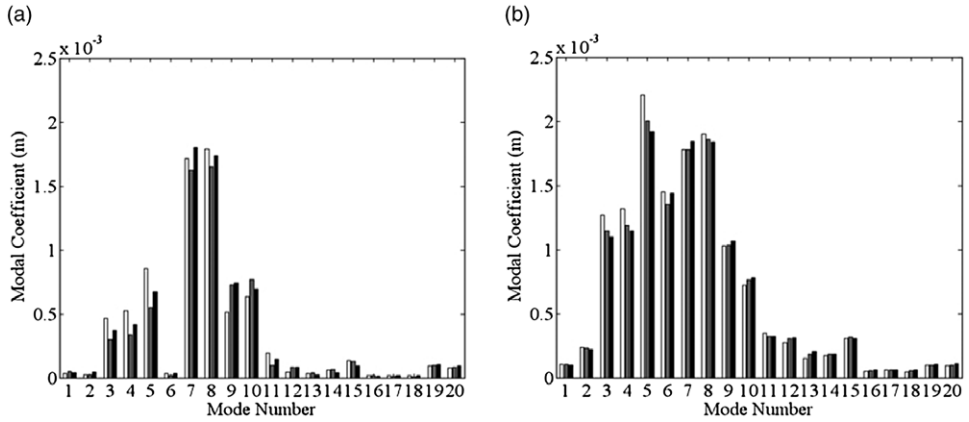

Figure 8. Modal contributions of the operational response of the wind turbine given the forcing functions illustrated in Figure 6 for (a) vertical wind shear, and (b) class B turbulence with wind shear for 8 (□), 10 (▒) and 14 m s^{-1} (■) mean wind speeds.

Figure 8 for the vertical wind shear case (Figure 8(a)) and turbulent wind case (Figure 8(b)). As anticipated, the turbulent wind state excited a broader range of modes of vibration than the vertical wind shear case. In particular, the dynamic response of the first symmetric flap mode of the rotor, mode #6, was nearly filtered out by the high pass filter in the case of vertical wind shear but this mode was strongly excited by turbulent wind broadband content. Because a certain type of damage would affect some of these modes of vibration more than others as explained in Figure 1, it was essential for SHM damage detection methods to take into account these variations in the forced response of the wind turbine. Both of these plots also indicated that the 14 modes of vibration were sufficient to describe the operational displacements experienced by the wind turbine.

3.2. Data acquisition and cleansing

Data acquisition and cleansing in the context of the Micon wind turbine began by considering measurement issues encountered when recording the wind speed from the anemometer tower. Cleansing was performed to mitigate the effects of bit dropout that occurred in this data. For this experiment, a rotor mounted data acquisition system transmitted data wirelessly to a base acquisition computer that merged the rotor data stream with data streams from the nacelle and inflow anemometer array. Unfortunately, the wireless access point and communication protocol were not able to guarantee the successful transmission and reception of the data packets resulting in the bit dropouts evident in the data. Figure 9(a) is a plot of the along-wind wind speed that clearly exhibited periods of time where the signal was lost. Figure 9(b) showed that these series of lost data resulted in autopower wind speed spectra over the 3 h period previously analysed in Figure 6(b). Based on these autopower spectra, which were corrupted by bias errors because of leakage, there was no evidence that the wind speed frequency content changed over the 3 h period. A sample-and-hold low-pass filter was used to fill gaps in the data because of the dropouts in Figure 9(a). After this filter was applied, the wind speed autopower spectra in Figure 9(c) were obtained. These spectra clearly indicated that the wind speed frequency content varied slightly over the 3 h period resulting in varying modal vibration amplitudes over that period.

Another critical data cleansing operation was the application of synchronous averaging to reduce the effects of leakage in the frequency spectra. For example, Figure 10 shows two autopower spectral estimates for the experimentally acquired flap acceleration obtained using synchronous averaging and overlap signal processing on data from the 6.5 m sensored blade low pressure side accelerometer. Two blocksizes were used that encompassed an integer number of rotations—one rotation and six rotations. It was clear from this result that at least six rotations were required to separate forced response components that were integer multiples of the 0.92 Hz rotor speed. An alternative to this form of synchronous averaging is angle domain signal processing, which also reduces leakage errors in frequency spectral estimates. Figure 11(a) illustrates how angle domain signal processing was applied to simulated force data like the data plotted in Figure 7. The force data halfway out along the blade from the simulation was tracked as a function of the azimuth angle of the rotor. Then this data was resampled to produce the same number of samples per rotation regardless of small changes in rotor speed. The frequency content of this resampled data was then plotted as shown in Figure 11(b) over many rotations and then averaged. The resulting average force history over one rotation of the rotor was then used to construct the distributions shown in Figure 7.

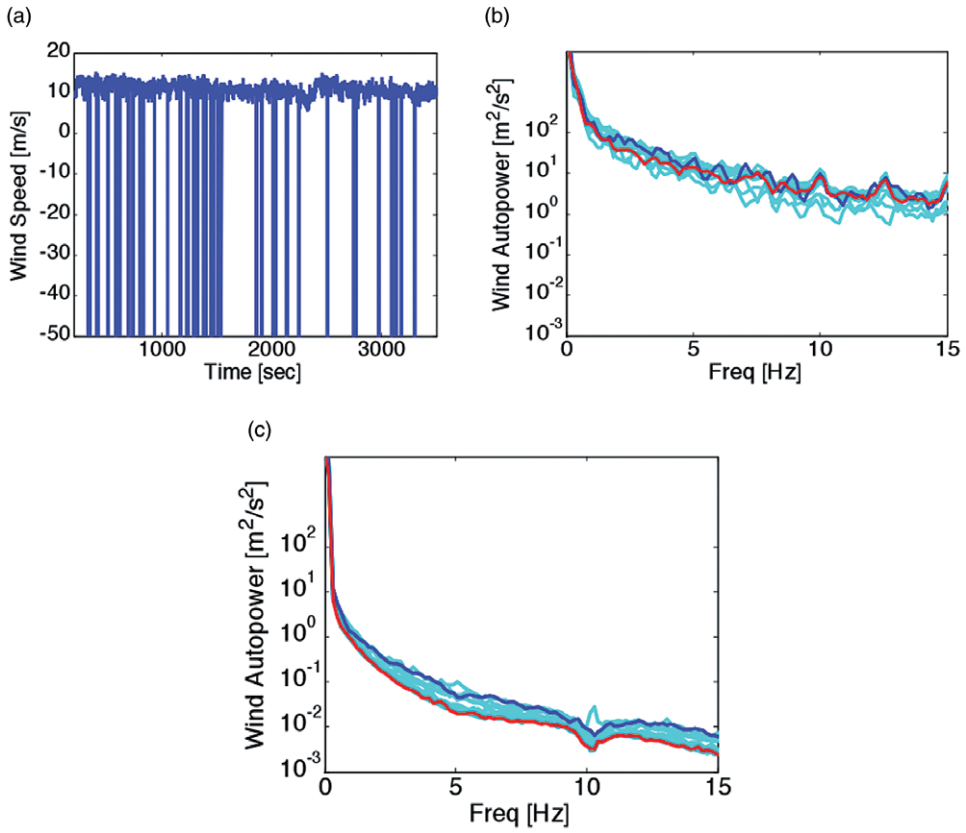

Figure 9. (a) Along-wind wind speed measurement at rotor height showing bit dropout (b) corresponding corrupted autopower spectral estimates using 50% overlap processing and Hanning window for 180 min period (—), initial 18 min (—), intermediate periods (—), and final 18 min (—); and (c) spectral estimates after sample and hold filter was applied to data in (a).

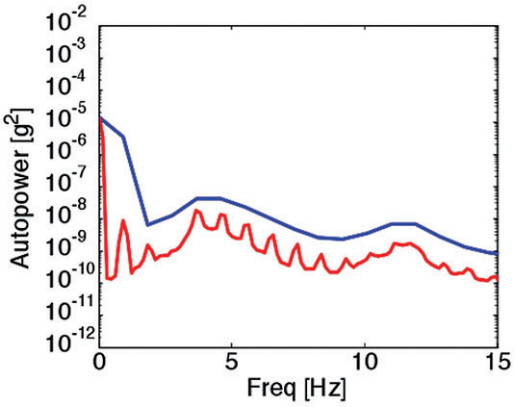

Figure 10. Experimentally measured autopower spectra of blade flap acceleration response at 6.5 m span position over 180 min period with 50% overlap processing and Hanning window using synchronous averaging with 1 (—) and 6 (—) rotor rotations.

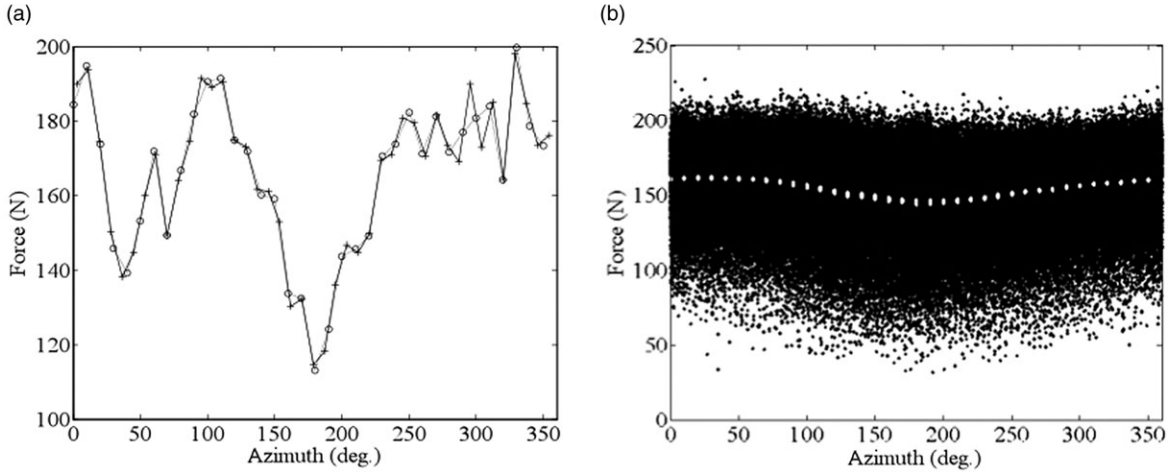

Figure 11. (a) Simulated force in flap direction on rotor blade at 5 m span position for one rotation in operation as a function of time sampling (+) and rotational sampling (O) and (b) many such cycles along with the averaged force (N).

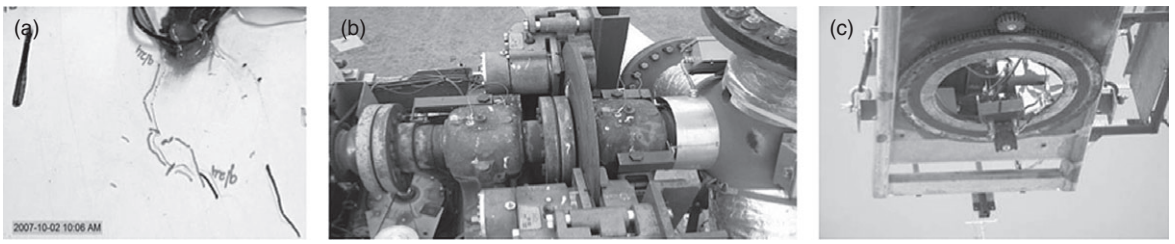

Figure 12. Components in which damage was simulated including (a) blade where crack in root area was modelled as a reduction in modulus consistent with an observation made in static blade test[11] (b) low-speed shaft where damage was modelled as a reduction in bending modulus and (c) yaw joint where damage was again modelled as a reduction in modulus.

3.3. Feature extraction

Feature extraction in the context of the Micon wind turbine began with an analysis of the sensitivity of the free vibration properties of the turbine to three types of damage. The free vibration properties include the natural frequencies and modal deflection shapes. Figure 12 shows the components that were modified in the simulation model to simulate mechanical damage. Damages in the blade root, low-speed shaft and yaw joint were simulated by reducing the bending stiffnesses in those areas by reducing the moduli of elasticity by 10, 25 and 50%. This approach was selected based on the discussion provided in Section 1.2.

The sensitivity of the natural frequencies to these three simulated damage mechanisms was quantified by calculating the percentage change, $\%_{baseline/damage}$, in all 14 undamped natural frequencies, $\omega_{n,damage}$, because of the reductions in stiffness using the baseline natural frequency, $\omega_{n,baseline}$, as the reference:

$$\%_{baseline/damage} = 100 \cdot \frac{\omega_{n,damage} - \omega_{n,baseline}}{\omega_{n,baseline}} \tag{5}$$

Figure 13 shows the percentage change in natural frequency for the 14 modes of vibration with respect to the corresponding damage mechanism in the blade, low-speed shaft and yaw joint. Each damage mechanism was simulated by a 25% reduction in the associated stiffness parameters. The largest percentage change in natural frequency was 3.6%. It is likely that the measured natural frequencies of a wind turbine would vary at least this much as a function of time of day. In addition, only a few of the natural frequencies of the wind turbine could be identified using transient operational data

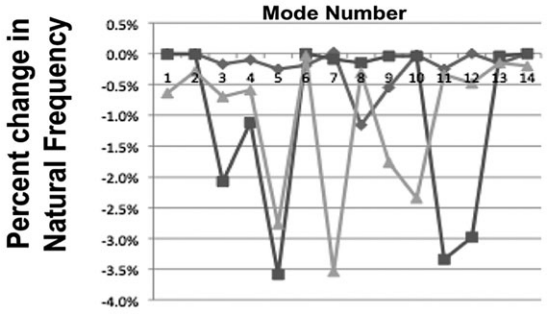

Figure 13. Percent reduction in natural frequencies of wind turbine simulation model for 25% reduction in stiffness in (a) blade root (◆), (b) low-speed shaft (▲) and (c) yaw joint (■).

during start-up; therefore, other features in the operational data were thought to be more fruitful in this investigation. Despite the small sensitivity of the natural frequency to the three damage mechanisms and the impracticality of using natural frequency as a feature for damage detection, this sensitivity chart revealed several important findings.

First, wind turbine natural frequencies were less sensitive to changes in the rotor blade than to changes in the yaw joint and low-speed shaft. This result suggested that to detect damage in the blade using only sensors integrated in the blade to measure the operational response, one would need to use a different feature than the natural frequency. Second, the sensitivity of each mode of vibration was significantly different for different damage mechanisms (as alluded to in Figure 1). For example, the natural frequency of the first mode of vibration involving fore-aft motion of the tower top was only sensitive to damage in the low-speed shaft and completely insensitive to the other two damages. Third, the sensitivity of a given natural frequency of vibration to a certain type of damage could be attributed to the modal deflection shape. Specifically, the degree to which the modal deflection shape 'exercised' a damaged component dictated the sensitivity of the corresponding natural frequency to the damage. For example, the fore-aft mode of vibration involved primarily a reactive moment produced by the rotor inertia causing the low-speed shaft to bend. Consequently, the natural frequency for the first mode of vibration was sensitive to damage in the low-speed shaft. Likewise, the natural frequency of the sixth mode of vibration corresponding to symmetric flap of the rotor blades was sensitive to damage in the blade root of one of the blades, but was insensitive to the other damages because there was no appreciable deflection of the low-speed shaft and yaw joint in this modal deflection shape. These results were important for SHM of the operating wind turbine because they indicate in which frequency range of the operating data one should focus in order to detect certain types of damages. In equation (1), changes to the natural frequencies in the denominators of the modal expansion terms would consequently change the forced response in operation.

A second damage feature considered was the MAC value for the modal deflection shapes. It is often found in SHM that localized damage of the type simulated in the blade, low-speed shaft and yaw joint in this paper is more easily detected using information derived from the modal deflection shapes. The MAC was calculated using the following expression:

$$MAC_{r,undamaged/damaged} = \frac{\{\psi_{r,undamaged}\}^T\{\psi_{r,damaged}\}}{\|\{\psi_{r,undamaged}\}\|\cdot\|\{\psi_{r,damaged}\}\|} \tag{6}$$

In this expression, the dot products between the modal vectors, $\{\psi_r\}$, for the cases when components were undamaged and damaged were calculated and normalized to produce a damage feature that varied between 0 (for dissimilar modal vectors) and 1 (for similar modal vectors). Figure 14 shows the results of this calculation for the 14 modes of vibration. One interesting result revealed by this feature was that the damage to one of the rotor blades only produced changes in the modal deflection shapes for modes 7 and 8. Recall from Figure 4 that these modal vectors corresponded to the first and second edge-wise modes of vibration of the rotor blades. Likewise, the simulated damage to the yaw joint primarily affected the modal deflection shapes for modes 3 and 4, which corresponded to the first rotor torsion and the first flap horizontal antisymmetric. These modal vectors resulted in significant moments acting across the yaw joint. Similarly, simulated damage to the low-speed shaft caused the most significant changes in the modal deflection shapes for modes 9 and 10, which corresponded to the second flap antisymmetric modes that produced moments across the low-speed shaft.

The features in Figures 13 and 14 were free vibration properties that would not be possible to identify in general using operational vibration data. Operational data could also be analysed using a modal decomposition such as the expression in equation (4). Figure 15 shows the results obtained after applying the procedure that was described following equation (4) to the simulated operational data under vertical wind shear in the case where blade damage was introduced in the root

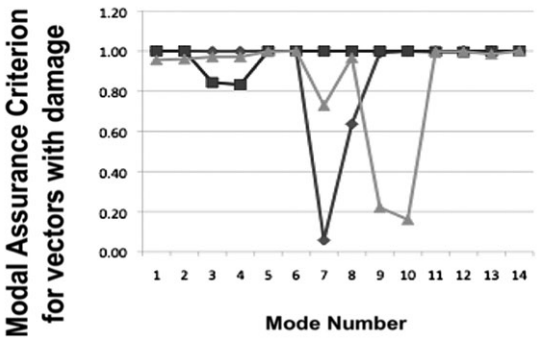

Figure 14. Modal assurance criterion of wind turbine simulation model for 25% reduction in stiffness in (a) blade root (♦), (b) low-speed shaft (▲), and (c) yaw joint (■).

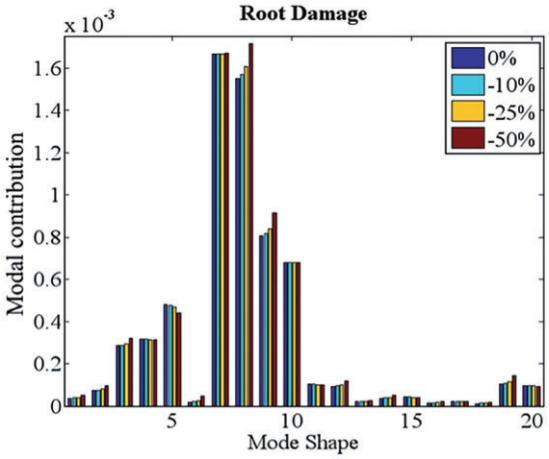

Figure 15. Modal contributions of the operational response of the wind turbine for a vertical wind shear wind state and force distribution in Figure 6(a) and various levels of simulated blade damage.

of the blade by reducing the stiffness by 10, 25 and 50%. These results yielded some conclusions about the sensitivity of the turbine operating vibrations to damage in the root of a blade. First, the sensitivities of the modal contribution to blade damage were correlated with the sensitivities of the natural frequencies to that type of damage. For example, modes 6, 8 and 9 exhibited relatively large sensitivities to blade damage in Figure 13. Likewise, these modes exhibited relatively high sensitivities to this type of damage in Figure 15. Although the contribution of the first symmetric flap mode of the rotor, mode #6, was small compared with other modes of vibration, it exhibited a 90% change in its modal contribution for the case of vertical wind shear for a 50% reduction in the blade stiffness. This result suggested that blade damage would be more readily observed for turbulent winds based on the results in Figures 8(a),(b). The other percent changes in modes 8 and 9, for instance, were on the order of 10–15% in magnitude. Second, Figure 15 indicated that it might have been possible to classify the type of damage that was present based on the pattern of changes that were observed in the modal contributions. Based on the sensitivity differences in the natural frequencies of vibration, it was hypothesized that different modal contributions would change for different types of damage for use classifying which type of damage had occurred, but more damage cases would need to be conducted to confirm this hypothesis

The damage features that were analysed above using natural frequencies and MAC values associated with the free response of the full wind turbine would be practical if sensors were installed across the turbine to enable the modal filter in equation (4) to be applied to operating data. These methods could also be applied to individual subsystems, i.e. only the rotor blades, to avoid the need for installing sensors across the full turbine.

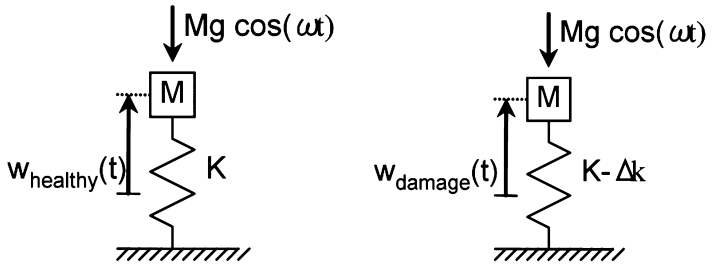

Figure 16. Simplified single degree of freedom model in the span direction for an oscillating gravitational load for the (a) undamaged and (b) damaged stiffness levels in the blade root.

An alternative method to the modal decomposition approach for extracting damage features was also considered in this work, which utilized the simplified model of a single degree of freedom oscillating subjected to an alternating gravitational load as illustrated in Figure 16(a). This degree of freedom was used to represent the blade's response in the span direction as it underwent cyclic gravitational loading. The deflection of the mass, M, which was the effective mass for the span-wise degree of freedom, was denoted by $w_{healthy}(t)$ and the nominal stiffness in the span-wise direction was denoted by K. After damage occurred in the root of the blade, this stiffness dropped to K-ΔK, and the displacement changed to $w_{damage}(t)$. The key assumption in this method for damage detection was that the gravitational loading, $Mg\cos(\omega t)$, did not change after damage occurred because this turbine was speed regulated leading to a constant ω and damage did not affect M or g. Structural damping was ignored in the model to simplify the feature extraction process. After writing the equations of motion for the healthy and damaged system models, the Fourier transform of each side of those equations were taken to produce equation 7(a),(b):

$$\frac{Mg}{\omega^2 M - K + \Delta k} = W_{damage} \tag{7a}$$

$$\frac{Mg}{\omega^2 M - K} = W_{healthy} \tag{7b}$$

where W_{damage} and $W_{healthy}$ indicate the dynamic displacements under cyclic gravitational loading. By combining equation 7(a),(b), the following damage index was obtained to quantify the reduction in stiffness because of damage:

$$\frac{\Delta k}{Mg} = \frac{W_{healthy} - W_{damage}}{W_{healthy} W_{damage}} = DI \tag{8}$$

The damage index was simply the normalized difference between the healthy and damaged dynamic displacement amplitudes in the span-wise direction of the blade.

This approach was applied to the simulation model under class B turbulent wind loading with vertical shear. In this simulation, the blade root stiffness for blade 1 was reduced by 10, 25 and 50%, and the damage index in equation (8) was calculated for all three blades using the dynamic displacement in the span-wise direction of the blades. The resulting damage indices were then plotted in Figure 17 for blades (a) 1 (b) 2 and (c) 3. Although there were a few areas in blades 1, 2 and 3 that indicated changes in stiffness, the area of blade 1 in which the stiffness had actually been reduced indicated a clear change in stiffness in the correct order from 10 to 25 to 50%. This damage index proved successful at both detecting and locating the reduction in stiffness in blade 1.

3.4. Statistical modelling

Statistical analysis was then conducted to determine if the changes that would be observed because of the types of damage simulated above would be significant enough to detect given the inherent variations in the wind loads. This type of comparative test is usually referred to as hypothesis testing. If the feature, x, was normalized according to the rule,

$$\frac{x - \mu}{\sigma} \tag{9}$$

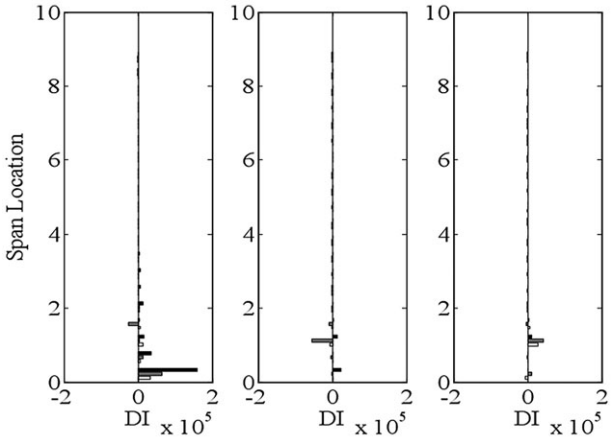

Figure 17. Simulated damage index calculated from equation (8) for blades (a) 1 (b) 2, and (c) 3 in class B turbulence showing increased damage from 10% (□) to 25% (▨) to 50% (■).

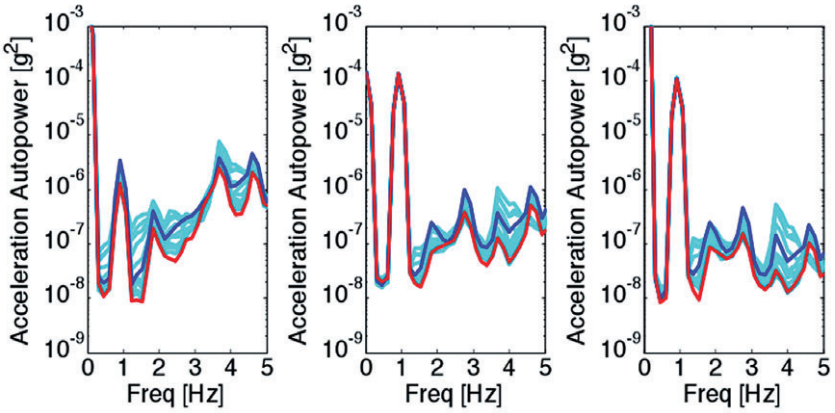

Figure 18. Experimentally measured acceleration autopowers at the 6.5 m blade span location over 3 h in the (a) flap (b) edge-wise, and (c) span directions using 50% overlap processing and Hanning window for 180 min period (—), initial 18 min (—), intermediate periods (—) and final 18 min (—).

where x was the feature, μ was its estimated mean and σ was its estimated standard deviation, then one's confidence in detecting that a statistically significant change had occurred in x could be quantified. For example, the modal contribution factures plotted in Figure 15 could serve as features x for hypothesis testing. Note that small deviations σ in x under normal circumstances would result in more readily detected changes because of damage because of the way in which equation (9) normalizes the change in x. To develop an understanding of which features studied in Section 3.3 would be most promising for damage detection, the experimentally measured operational accelerations for the Micon turbine were used to estimate and plot the autopowers for the flap, edge-wise and span directions of the instrumented blade in Figure 18 by applying the same method that was used in Figure 6(b) and Figure 10. The first five harmonics were evident in Figure 18. It was noted that the flap direction acceleration exhibited much more variation over the 3 h period in which data was acquired than the edge-wise and span direction accelerations. The reason that the variations were less in the edge-wise and span direction measurements was because the primary forcing function at 1 per revolution (0.92 Hz) in these directions was due to gravity. As previously mentioned in the discussion surrounding Figure 16, the gravitational force was nearly constant for this speed regulated wind turbine. This result suggested that it would be feasible to detect damage in the wind turbine using the measured responses at 1 per revolution because the edge-wise and span direction measurements exhibited smaller σ values (see equation (9)). Figure 18 also indicated the deviation that each of these spectra exhibited at the various harmonics of the rotor speed.

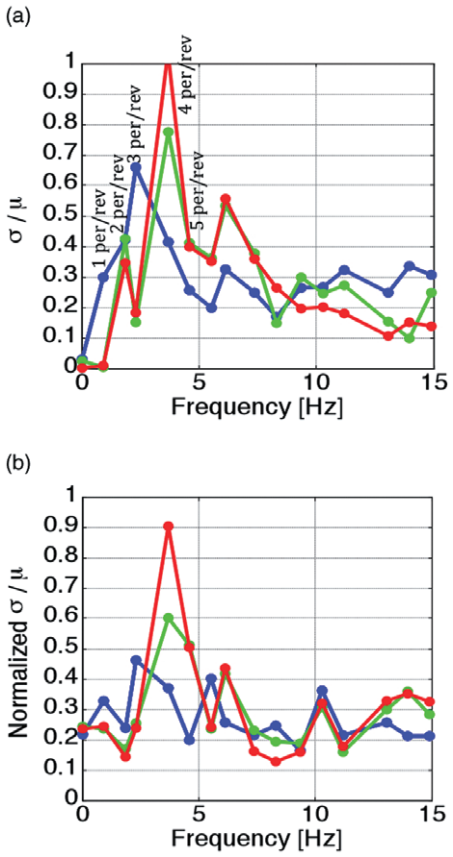

Figure 19. Experimentally measured normalized standard deviation in the flap (—), edge-wise (—), and span (—) directions at the 6.5 m blade span location (a) without and (b) with wind speed normalization included.

To develop a better understanding of how the standard deviation was changing relative to the mean of the corresponding spectral amplitude value, Figure 19 was plotted by extracting the mean amplitudes and standard deviations at 0 Hz, 0.92 Hz, and several harmonics of the rotor speed. This plot clearly indicated the benefit of using the response data at 0.92 Hz because of the small normalized variations in amplitude at this frequency. The variations in all of the responses at 0 Hz were also small suggesting that these quasi-static responses could be useful for change detection. The variations at harmonics of the rotor speed were significantly larger suggesting that greater changes would need to be observed in these spectral amplitudes to identify a statistically significant change in the operating response because of damage. To quantify the change in any one of these measured spectral amplitudes that would be required to detect changes because of damage, x in equation (9) was assumed to be equal to $\mu \pm 3\sigma$. This level of change from the mean value of x would correspond to a 99% confidence interval, meaning that the analyst would be 99% certain that this level of change in x would correspond to a biased change in the feature even amidst the natural variations in x. When this substitution was made in equation (9), the following expression was obtained after some manipulation:

$$\left|\frac{x}{\mu} - 1\right| = \frac{3\sigma}{\mu} \tag{10}$$

This expression was used to calculate how much of a shift in x would be required to detect a change in x with 99% confidence. For example, the span direction acceleration autopower in Figure 19 at 1 per revolution exhibited a σ/μ of 0.01 resulting in a required percent change in x of 3% to achieve a 99% confidence in the diagnosis that a change (because of damage) occurred in the wind turbine. Likewise, the flap direction acceleration autopower from Figure 19 at 1 per revolution would be required to change by 90% to achieve a 99% confidence that a change occurred because of damage. An attempt was made to normalize the acceleration autopower to reduce these inherent variations in the flap acceleration because of wind loads. When the autopowers in Figure 18 were normalized by the wind speed autopower in Figure 6(b),

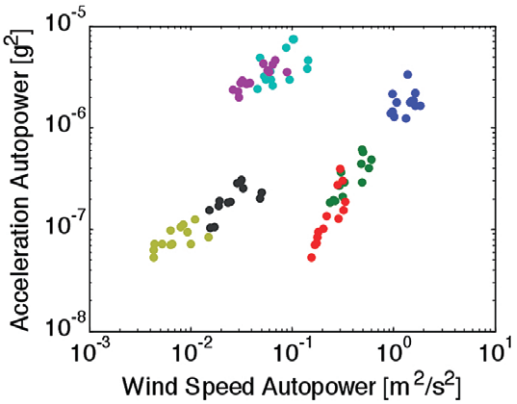

Figure 20. Experimentally measured acceleration autopowers at 0.92 Hz (●) and its first six harmonics (●,●,●,●,●,●) plotted versus wind speed autopower.

the plot in Figure 19(b) was obtained. Note that the variation worsened at 0 Hz and 1 Hz for reasons that are not yet understood; however, the variation was reduced in the flap direction as was anticipated at 2 per revolution, 3 per revolution and 5 per revolution when compared with Figure 19(a). For example, the required percent change in the flap acceleration autopower was 75% at 5 per revolution, but the percent change required in the flap acceleration when normalized by the wind speed was only 60% to achieve 99% confidence in the diagnosis that change occurred. The changes in the modal contributions plotted in Figure 15 near the first mode (close to 1 per revolution) reach 30%, near the sixth mode (close to 6 per revolution) reach 100% and near the eighth and ninth modes (close to 8 and 9 per revolution) reach 25%. Based on a comparison of the modal sensitivity to the normalized standard deviation in Figure 19(a), it was concluded that the changes in the modal contributions plotted in Figure 15 would be large enough to detect amidst the natural variations in the operation of the Micon turbine at 1 per revolution (in the edge-wise and span directions), at 6 per revolution (in all three directions especially the flap direction) and at 9 per revolution (in edge-wise and flap directions). If the data was normalized by the along-wind wind speed as in Figure 19(b), changes could also be detected within the variation of the turbine operation in the span direction at other harmonics.

To understand how to better normalize the acceleration response to reduce the effects of the variations in wind speed, the acceleration autopower magnitudes at 0.92 Hz and its first six harmonics were plotted versus the corresponding wind speeds at those frequencies in Figure 20. This plot indicated that there was a discernible linear correlation between changes in acceleration and changes in wind speed for the 2 per revolution, 3 per revolution, 5 per revolution and higher frequencies because the data points at these frequencies followed a straight line, but the correlations at 1 per revolution and 4 per revolution were not as evident because the data points at these frequencies fell into clusters. This type of two element feature vector could be considered in the future for use in damage detection, but more simulation modelling and testing would need to be conducted to determine if the method would be effective for damage detection.

4. CONCLUSIONS

The SHM process was described as a problem in statistical pattern recognition for HAWTs wind turbines in operation. An updated turbine simulation model was used to study the operational response under both vertical wind shear and turbulent wind conditions to reveal changes in the operating vibration response because of these changes in wind loads. It was shown through a sensitivity analysis of the natural frequencies of vibration to three types of damage in the blade, low-speed shaft and yaw joint that these changes in wind loads led to a change in the sensitivity of the operating vibrational response of the wind turbine to the damage being detected. It was also shown that there was less than a 4% change in the wind turbine natural frequencies given a 25% reduction in the stiffness at the root of one blade. The MAC exhibited significant changes because of the three simulated damage scenarios; therefore, the modal contributions were estimated using a modal decomposition approach to produce features for damage detection. Large changes from 10–100% in these root mean square modal contribution coefficients were observed for 50% reductions in blade root stiffness. By studying the statistics of experimentally acquired data from the operating wind turbine, it was demonstrated that the standard deviation was smallest for the span and edge-wise measurements at 1 per revolution because of consistency of the gravitational force at this frequency. Only a 3% change in the response in the span and edge-wise directions because

of damage was required to detect a change with 99% confidence in contrast with the 90% change in flap direction response that was required to detect a similar change because of damage. The dynamic displacement in the span direction was also proven to be useful for damage detection. This feature was formed by normalizing the difference between the dynamic displacements in the span direction and was shown to both locate and quantify the reduction in stiffness in the blade root.

REFERENCES

1. Walford CA. Wind Turbine Reliability: Understanding and Minimizing Wind Turbine Operation and Maintenance Costs. 2006. Sandia Report, SAND2006-1100.
2. Hahn B, Durstewitz M, Rohrig K. *Reliability of Wind Turbines*. Wind Energy, Springer Berlin Heidelberg: New York, 2007; 329–332.
3. Ciang CC, Lee J-R, Bang H-J. Structural health monitoring for a wind turbine system: a review of damage detection methods. *Measurement Science Technology* 2008; **19**: 1–20.
4. Adams DE. *Health Monitoring of Structural Materials and Components*. John Wiley & Sons: Chichester, U. K., 2007.
5. Boller C, Chang F-K, Fujino Y. (eds). *Encyclopedia of Structural Health Monitoring*. John Wiley & Sons: Chichester, U. K., 2009.
6. Byrne G, Dornfeld D, Inasaki I, Ketteler G, Konig W, Teti R. Tool condition monitoring (TCM)—the status of research and industrial application. *CIRP Annals—Manufacturing Technology* 1995; **44**: 541–567.
7. Tandon N, Choudhury A. A review of vibration and acoustic measurement methods for the detection of defects in rolling element bearings. *Tribology International* 1999; **32**: 469–480.
8. Singh GK, Al Kazzaz SAS. Induction machine drive condition monitoring and diagnostic research—a survey. *Electric Power Systems Research* 2003; **64**: 145–158.
9. White J, Adams D, Rumsey M, Zayas J. *Measurement of Operational Loading and Deflection with a Smart Turbine Rotor Blade*. Windpower: Chicago, IL, 2009.
10. Park G, Farrar C, Lanza di Scalea F, Coccia S. Performance assessment and validation of piezoelectric active-sensors in structural health monitoring. *Smart Materials and Structures* 2006; **15**: 1673–1683.
11. White J, Adams D, Rumsey M, van Dam J, Hughs S. Impact loading and damage detection in a carbon composite TX-100 wind turbine rotor blade. *Proceedings of the AIAA Aerospace Sciences Meeting and Exhibit*, Denver, CO, 2008.
12. Lading L, McGugan M, Sendrup P, Rheinlander J, Rusborg J. Fundamentals for Remote Structural Health Monitoring of Wind Turbine Blades—a Preproject: Annex B—Sensors and Nondestructive Testing Methods for Damage Detection in Wind Turbine Blades. 2002. RisØ-R-1341 (EN).
13. Drewry MA, Georgiou GA. A review of NDT techniques for wind turbines. *Insight* 2007; **49**: 137–141.
14. Kusiak A, Zheng H, Song Z. Models for monitoring wind farm power. *Renewable Energy* 2009; **34**: 583–590.
15. Aykul H, Ediz IG, Akcakoca H, Erarslan K, Taksuk M, Dixon-Hardy DW. Statistical process control for coal fired power plant system. *Journal of the Energy Institute* 2010; **83**: 41–47.
16. Jones P, Sutherland H, Neal B. LIST/BMI Turbines Instrumentation and Infrastructure. 2001. Sandia Report, SAND2001-1642.
17. Sohn H, Farrar C, Hunter N, Worden K. Structural health monitoring using statistical pattern recognition techniques. *Journal of Dynamic Systems, Measurement, and Control* 2001; **123**: 706–711.
18. Worden K, Manson G. The application of machine learning to structural health monitoring. *Philosophical Transactions of the Royal Society of London Series A* 2007; **365**: 515–537.
19. Liu W, Tang B, Jiang Y. Status and problems of wind turbine structural health monitoring techniques in China. *Renewable Energy* 2009; **35**: 1414–1418.
20. Ghoshal A, Sundaresan MJ, Schulz MJ, Pai FP. Structural health monitoring techniques for wind turbine blades. *Journal of Wind Engineering and Industrial Aerodynamics* 2000; **85**: 309–324.
21. Sundaresan MJ, Schulz MJ, Ghoshal A. Structural health monitoring static test of a wind turbine blade. 2002, NREL/SR-500-28719.
22. Krikera G, Shinde V, Schulz M, Sundaresan M, Hughes S, van Dam J, Nkrumah F, Grandhi G, Ghoshal A. Monitoring multi-site damage growth during quasi-static testing of a wind turbine blade using a structural neural system. *Structural Health Monitoring* 2008; **7**: 157–173.
23. Hyers RW, McGowan JG, Sullivan KL, Manwell JF, Syrett BC. Condition monitoring and prognosis of utility scale wind turbines. *Energy Materials* 2006; **1**: 187–203.

24. Corey P, Grisso B, Inman D. Impedance-based structural health monitoring of wind turbine blades. *Proceedings of SPIE* 2007; **6532**: 65321I-1–65321I-11. Health Monitoring of Structural and Biological Systems.
25. Rumsey M, Paquette J. Structural Health Monitoring of Wind Turbine Blades. *Proceedings of the SPIE* 2008; **6933**: 69330E-1–69330E-15. SPIE-2008-6933-14A.
26. Schroeder K, Ecke W, Apitz J, Lembke E, Lenschow G. A fibre Bragg grating sensor system monitors operational load in a wind turbine rotor blade. *Measurement Science and Technology* 2006; **17**: 1167–1172.
27. Walford CA, Roberts D. *Condition Monitoring of Wind Turbines: Technology Overview, Seeded-Fault Testing, and Cost-Benefit Analysis*. EPRI: Palo Alto, CA, 2006; 1010419.
28. Hameed Z, Hong YS, Cho YM, Ahn SH, Song CK. Condition monitoring and fault detection of wind turbines and related algorithms: a review. *Renewable and Sustainable Energy Reviews* 2009; **13**: 1–39.
29. White J, Adams D, Rumsey M. Modal Analysis of CX-100 Rotor Blade and Micon 65/13 Wind Turbine. *Proceedings of the International Modal Analysis Conference*, Jacksonville, FL, 2010.
30. Simmermacher T, Carne T. *'Tower Modal Survey.'* Internal Memo, Albuquerque, New Mexico: Sandia National Laboratories, 1999.
31. Saranyasoontorn K, Manuel L, Veers PS. *'On Estimation of Coherence in Inflow Turbulence based on Field Measurements',* AIAA, 23rd ASME Wind Energy Symposium, Reno, Jan 2004.